

Low-Temperature Magnetic Force Microscopy on Single Molecule Magnet-Based Microarrays

Michele Serri, Matteo Mannini, Lorenzo Poggini, Emilio Vélez-Fort, Brunetto Cortigiani, Philippe Sainctavit, Donella Rovai, Andrea Caneschi, Roberta Sessoli

▶ **To cite this version:**

Michele Serri, Matteo Mannini, Lorenzo Poggini, Emilio Vélez-Fort, Brunetto Cortigiani, et al.. Low-Temperature Magnetic Force Microscopy on Single Molecule Magnet-Based Microarrays. Nano Letters, 2017, 17 (3), pp.1899-1905. 10.1021/acs.nanolett.6b05208 . hal-03989116

HAL Id: hal-03989116
https://cnrs.hal.science/hal-03989116

Submitted on 14 Feb 2023

HAL is a multi-disciplinary open access archive for the deposit and dissemination of scientific research documents, whether they are published or not. The documents may come from teaching and research institutions in France or abroad, or from public or private research centers.

L'archive ouverte pluridisciplinaire **HAL**, est destinée au dépôt et à la diffusion de documents scientifiques de niveau recherche, publiés ou non, émanant des établissements d'enseignement et de recherche français ou étrangers, des laboratoires publics ou privés.

Low temperature magnetic force microscopy on single molecule magnet-based microarrays

Michele Serri,[1,2] *Matteo Mannini,*[1,2]* *Lorenzo Poggini,*[1,2†]

Emilio Vélez-Fort,[3] *Brunetto Cortigiani,*[1,2] *Philippe Sainctavit,*[4]

Donella Rovai,[1,2] *Andrea Caneschi,*[1,2] *Roberta Sessoli*[1,2]

[1] Laboratory for Molecular Magnetism (LA.M.M.), Department of Chemistry "Ugo Schiff", Università degli Studi di Firenze via della Lastruccia 3-13, I-50019 Sesto Fiorentino, Italy.

[2] INSTM Research Unit of Firenze, via della Lastruccia 3, I-50019 Sesto Fiorentino, Italy.

[3] European Synchrotron Radiation Facility, 71 Av. Martyrs, F-38043 Grenoble 9, France

[4] Institut de Mineralogie, de Physique des Materiaux et de Cosmochimie, UMR 7590, CNRS, UPMC, IRD, MNHN, F-75005 Paris, France & Synchrotron SOLEIL, L'Orme des Merisiers, Saint-Aubin—BP 48, F-91192 Gif-sur-Yvette, France

ABSTRACT

The magnetic properties of some single molecule magnets (SMM) on surfaces can be strongly modified by the molecular packing in nanometric films/aggregates or by interactions with the substrate, which affect the molecular orientation and geometry. Detailed investigations of the magnetism of thin SMM films and nanostructures are necessary for the development of spin-

based molecular devices, however this task is challenged by the limited sensitivity of laboratory based magnetometric techniques and often requires access to synchrotron light sources to perform surface sensitive X-ray magnetic circular dichroism (XMCD) investigations. Here we show that low temperature magnetic force microscopy (LT-MFM) is an alternative powerful laboratory tool able to extract the field dependence of the magnetization and to identify areas of in-plane and perpendicular magnetic anisotropy in microarrays of the SMM Terbium(III) bis-phthalocyaninato ($TbPc_2$) neutral complex grown as nanosized films on SiO_2 and Perylene-3,4,9,10-tetracarboxylic dianhydride (PTCDA), in agreement with data extracted from non-local XMCD measurements performed on homogeneous $TbPc_2$/PTCDA films.

KEYWORDS. Magnetic Force Microscopy; molecular magnetism; magnetic anisotropy; patterning; dipolar field ; Terbium double decker

MAIN TEXT

Single molecule magnets (SMM) are magnetic systems featuring slow relaxation of the magnetization at low temperature that gives rise to a dynamic hysteretic behavior; this effect is coupled with the occurrence of resonant quantum tunneling mechanism that widen the potential interest of those objects for the development of novel molecular spintronics devices.[1–3] Recent research efforts have been directed towards the organization of SMM units onto surfaces,[4–6] which represents a milestone for the realization of solid state devices. The interaction with the surface can affect molecular packing and orientation, significantly modifying the magnetic response of a molecular film. Magneto-optical techniques,[7,8] in particular X-ray magnetic circular dichroism (XMCD),[9,10] are the most employed techniques to characterize thin films, the

latter achieving sub-monolayer sensitivity but requiring the access to special facilities (synchrotron light sources). If spatial resolution is also required, such as in sub-micrometric devices, scanning probe techniques can be employed. Spin polarized STM[11–13] and inelastic electron tunneling spectroscopy (IETS)[14,15] have provided detailed information on magnetic properties of isolated magnetic molecules on surfaces but they require very demanding experimental conditions and instrumentation.

Magnetic force microscopy (MFM) is an affordable technique to probe the local magnetization of materials and can access information at nanometric length scales that are relevant for molecular spintronic devices, offering superior spatial resolution compared to scanning superconducting quantum interference device (SQUID) and scanning Hall probe microscopy.[16,17] MFM has been extensively used to study, as well as to manipulate, the domain structure of ferromagnetic inorganic films[18–20] and micro- or nano-structures,[21–23] or vortexes in superconductors.[24–26] The application of this technique to molecular magnetic materials is however largely unexplored and most of the studies in the literature are limited to room temperature and lack a systematic field dependent characterization at low temperature,[27–30] which is necessary to evaluate the magnetic properties of the material and rule out topographic or electrostatic spurious contributions to the MFM measurement.

Notable exceptions are the recent report of Lorusso *et al.* where MFM has been used to extract the low temperature magnetization curve of micrometric aggregates of a paramagnetic gadolinium acetate complex,[31] or that of Pinilla-Cienfuegos *et al.*, who have investigated the magnetic switching of ferromagnetic ($T_c \approx 40$ K) Prussian blue analogue (PBA) nanoparticles of different sizes.[32,33] PBA nanoparticle patterns were also magnetically imaged at low temperature

using scanning hall probe microscopy by Ghirri *et al*.[34] To the best of our knowledge there are no reported examples of MFM characterization of a SMM system at low temperature.

In this work we demonstrate that a carefully prepared nanostructure of Terbium(III) bis-phthalocyaninato neutral complex ($TbPc_2$ hereafter) can be characterized using MFM, obtaining a local magnetization curve and an unprecedented lateral resolution of the dipolar field distribution of the molecular nanostructures. $TbPc_2$ (Figure 1a) is a single ion-based SMM with large total angular momentum, J=6, and a strong magnetic anisotropy with the easy axis of magnetization perpendicular to the planes of the phthalocyaninato ligands. Thanks to its stability it can be thermally sublimed to a variety of substrates, often maintaining the SMM behavior[9,35,36] or being influenced by specific magnetic substrates.[3,37]

In this study we have also profited of the possibility to control the molecular orientation in the film by tuning the molecule-substrate interactions. Weakly interacting materials and amorphous or rough surfaces favor a standing orientation of the phthalocyaninato rings, where the easy axis lies parallel to the film. This characteristic would be disadvantageous for the realization of spintronic devices and it is not ideal for MFM measurements, since the easy axis is generally oriented in random directions in the plane of the film, suppressing the net magnetic moment of the sample and potentially reducing effects such as magnetoresistance.[38] In order to prepare an optimized sample for a LT-MFM characterization (see Supporting Information, SI hereafter, for details of samples preparation), we deposited the SMMs-on a templating agent[39] constituted by a thin film of Perylene-3,4,9,10-tetracarboxylic dianhydride (PTCDA, Figure 1b), which is known to induce a planar orientation of phthalocyanine molecules. This approach has been earlier adopted for $TbPc_2$ by the group of Salvan[40] that reported an enhancement at room temperature of the magnetic circular dichroism of this molecule when deposited on PTCDA

compared to SiO_2/Si substrates. More recently, by combining Cantilever Torque Magnetometry (CTM) and X-Ray Natural Linear Dichroism (XNLD), some of us[41] showed that $TbPc_2$ films deposited on PTCDA are strongly ordered with the phthalocyanine (Pc) plane parallel to the surface resulting in out-of-plane magnetic anisotropy that is maintained in samples several tens of nm thick.

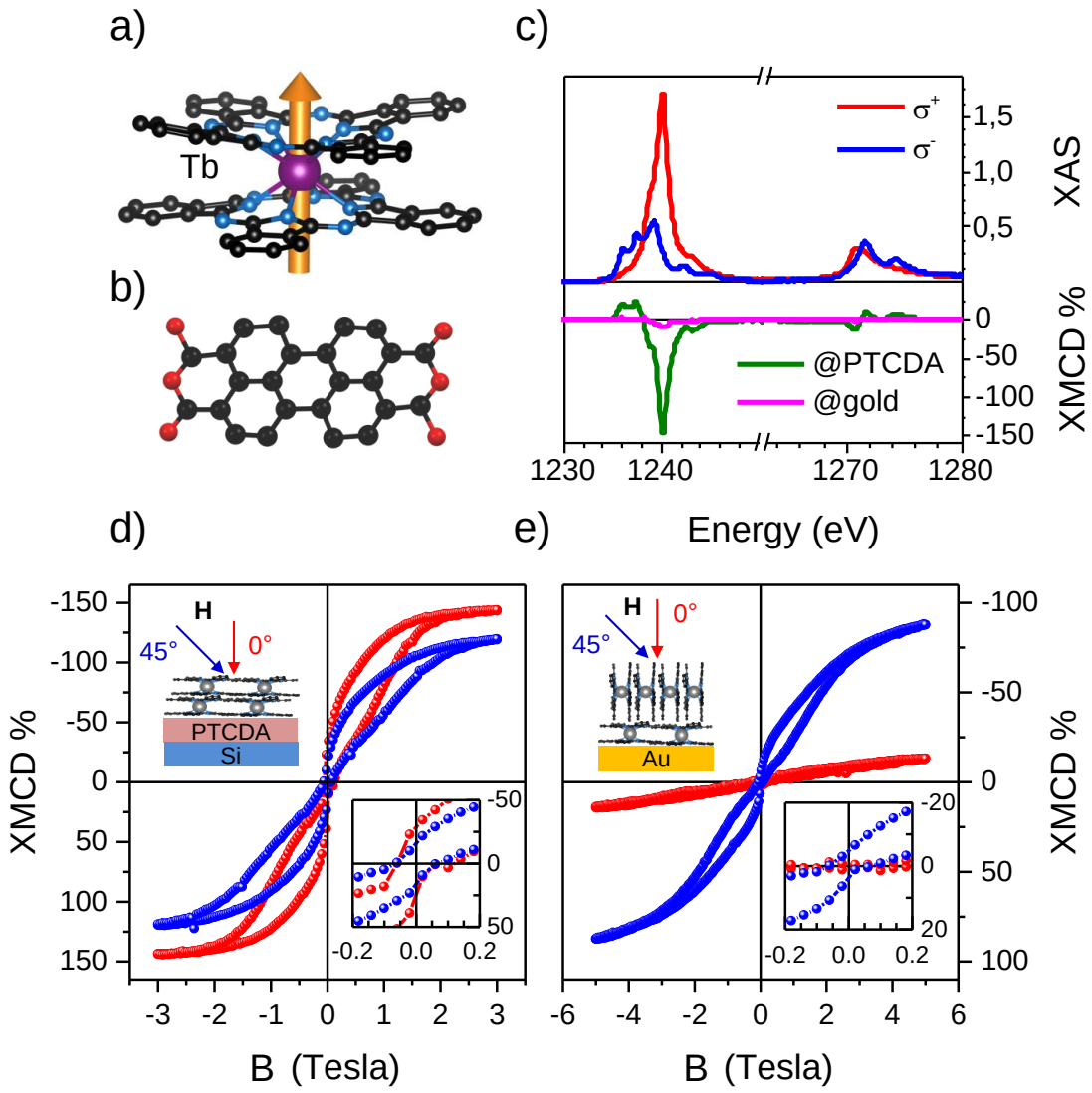


Figure 1 a) $TbPc_2$ molecule; carbon atoms are shown in black, nitrogen in blue, terbium in purple, hydrogen atoms are not shown. The orange arrow represents the *J*=6 total angular

momentum aligned along the easy axis. b) PTCDA molecule, with oxygen atoms shown in red. c) X-ray absorption spectra of right (red line) and left (blue line) polarized light in a 20 nm $TbPc_2$ film on PTCDA (20 nm) on silicon, measured at 7 K and B=3 T at normal incidence. The resulting XMCD spectrum measured at normal incidence is shown in green and compared to the XMCD of a 100 nm $TbPc_2$ film on bare gold (pink line) measured in the same conditions. d) XMCD hysteresis curves of the 20 nm $TbPc_2$/PTCDA film at normal (red dots) and 45° incidence (blue dots); the inset shows the opening of the hysteresis at B=0 T. e) XMCD hysteresis curve of the 100 nm $TbPc_2$/Au film at normal (red dots) and 45° incidence (blue dots); the inset shows the smaller opening of the hysteresis at B=0 T compared to the film on PTCDA.

Prior to a local characterization of these samples, in order to allow a detailed comparison of the MFM features and the magnetic and hysteretic behavior of $TbPc_2$ at the nanoscale, we performed a characterization of the angular dependence of the magnetic hysteresis of $TbPc_2$ films on different substrates using circularly polarized X-ray synchrotron radiation at the ID32 beamline at ESRF synchrotron.[42] The upper part of Figure 1c shows the absorption spectra of circularly polarized X-rays measured at 7 K at the $M_{4,5}$ Tb edge in a 20 nm $TbPc_2$ film on a 20 nm PTCDA layer with a magnetic field of 3 Tesla oriented normal to the sample (θ=0°). The lower part of Figure 1c compares the normal incidence X-ray circular magnetic dichroism (XMCD) spectra of this sample with a thick $TbPc_2$ (100 nm) film on polycrystalline gold. The dichroism detected at normal incidence (θ=0°) on the topmost layers of a relatively thick film of $TbPc_2$ on PTCDA, expected with preferential orientation of the easy axis perpendicular to the film, is larger than then the dichroism of the thick film deposited on gold. Topmost layers of this deposit contain $TbPc_2$ molecules sitting in standing configuration analogously to thick films on aluminum foil.[35] These evidences are consistent with the results of our recent investigation of these materials by

CTM and XNLD.[41] The dichroic ratio is therefore strongly enhanced in the film grown on PTCDA, reaching a maximum at E=1240 eV close to 150% of the isotropic XAS. This result is comparable with the XMCD previously measured in $TbPc_2$ monolayers on gold[35] in which molecules are known to have a flat orientation of the phthalocyanine ring.[43]

Following the XMCD experiments, we measured the magnetic hysteresis loops of the two samples at the two orientations by recording the field dependence of the XMCD at the energy of the maximum dichroism (1240 eV). The sample on PTCDA (Figure 1d) shows an open hysteresis loop with the characteristic butterfly shape of the $TbPc_2$ single molecule magnet, which is caused by the high spin relaxation rate at zero applied field due to resonant quantum tunneling. The hysteresis is remarkably wider that previously observed in monolayers on gold,[35] which is partly due to the different experimental conditions (temperature and field sweep rate that strongly alter the SMM behavior) but can also indicate a slower relaxation rate on PTCDA compared to the monolayer on gold, analogously to what has been recently found by Dreiser *et al.* on MgO.[44] At θ=45° the magnetic moment is reduced due to the Tb anisotropy. In the thick film on gold (Figure 1e), the hysteresis opening is greatly reduced at θ=45°, while in the hard direction (θ=0°), the magnetic moment is almost suppressed and the hysteresis is negligible.

The different molecular orientation and magnetic response of $TbPc_2$ molecules on different substrates was then exploited in a multiple shadow masking process to generate a superstructure of arrays of microdots with different (in-plane and out-of-plane) magnetic anisotropy. If patterning is a necessary step to create a topographic and magnetic profile easily detected in scanning force microscopy, the original superstructure we designed here further enhances the magnetic contrast by allowing a direct comparison between identical topographic structures with expected different magnetic signal. We deposited PTCDA by sublimation through a 2000 mesh

Cu TEM grid, with square holes 7.5 μm wide spaced by 5 μm, in contact with a silicon substrate. Subsequently, a pattern of $TbPc_2$ dots was created with a smaller TEM grid, consisting of Cu grids (200 mesh) covered by a carbon film perforated in a regular pattern of circular holes with 1.2 μm diameter and 1.3 μm separation. We notice that $TbPc_2$ is expected to maintain their orientation on both PTDA and Si independently to the thickness of the deposit.[41] The topography of the structures was checked with atomic force microscopy (AFM) at room temperature and during the MFM measurement at low temperature (Figure 2a) revealing an array of $TbPc_2$ dots with a truncated cone shape of average height of 24 nm and half-height diameter of 1.7 μm, distributed over PTCDA squares of 12 nm height.

The $TbPc_2$/PTCDA structures were cooled down to a temperature of 10 K in a field of 4 Tesla and studied with MFM, configured with a phase locked loop (PLL) feedback on the cantilever oscillation and a dual pass measurement where each line of the image is scanned twice, the first time tapping the surface to record the topography and the second at a lift height of 85 nm from the sample and following the firstly acquired profile to isolate long range magnetic interactions from the morphology contribution. In the PLL mode, the magnetic contrast is measured as the shift f of the cantilever resonance frequency from a reference value; here f was set to 0 at the center of the dot on PTCDA. High coercivity MFM probes (ASYMFMHC, nominal H_c~0.5 T/μ_0 at room temperature) were used in the experiment.

Figure 2b shows the MFM signal measured at 10 K applying an out-of-plane field of 4 T on a 12.6 × 12.6 μm^2 area containing both $TbPc_2$ dots on PTCDA and on bare silicon, as highlighted by the topography image in Figure 2a simultaneously acquired. The MFM image shows a sharp difference of the magnetic contrast between $TbPc_2$ structures grown on differently

treated substrate areas, which can also be appreciated in the frequency shift profiles presented at the bottom of Figure 2b. As expected, the dots on the templating agent show the largest magnetic contrast due to the perpendicular orientation of the $TbPc_2$ easy axis, while the dots on silicon exhibit much lower net magnetization due to the unfavorable in-plane orientation of the easy axis. The magnetic origin of the measured signal was confirmed by measurements in zero field, after performing a demagnetizing sequence, which showed negligible contrast (data in Figure S2 and Figure S4 in SI). Interestingly, MFM imaging of the dots grown across the boundaries of the PTCDA squares show the transition of the magnetic anisotropy from one orientation to the other within the same dot. This demonstrates the capability of the MFM measurement to perform a local magnetic characterization on a scale significantly smaller than the size of the dots. Furthermore, it shows how neighboring film domains of different orientation are magnetically uncoupled, which is a consequence of the paramagnetic nature of $TbPc_2$.

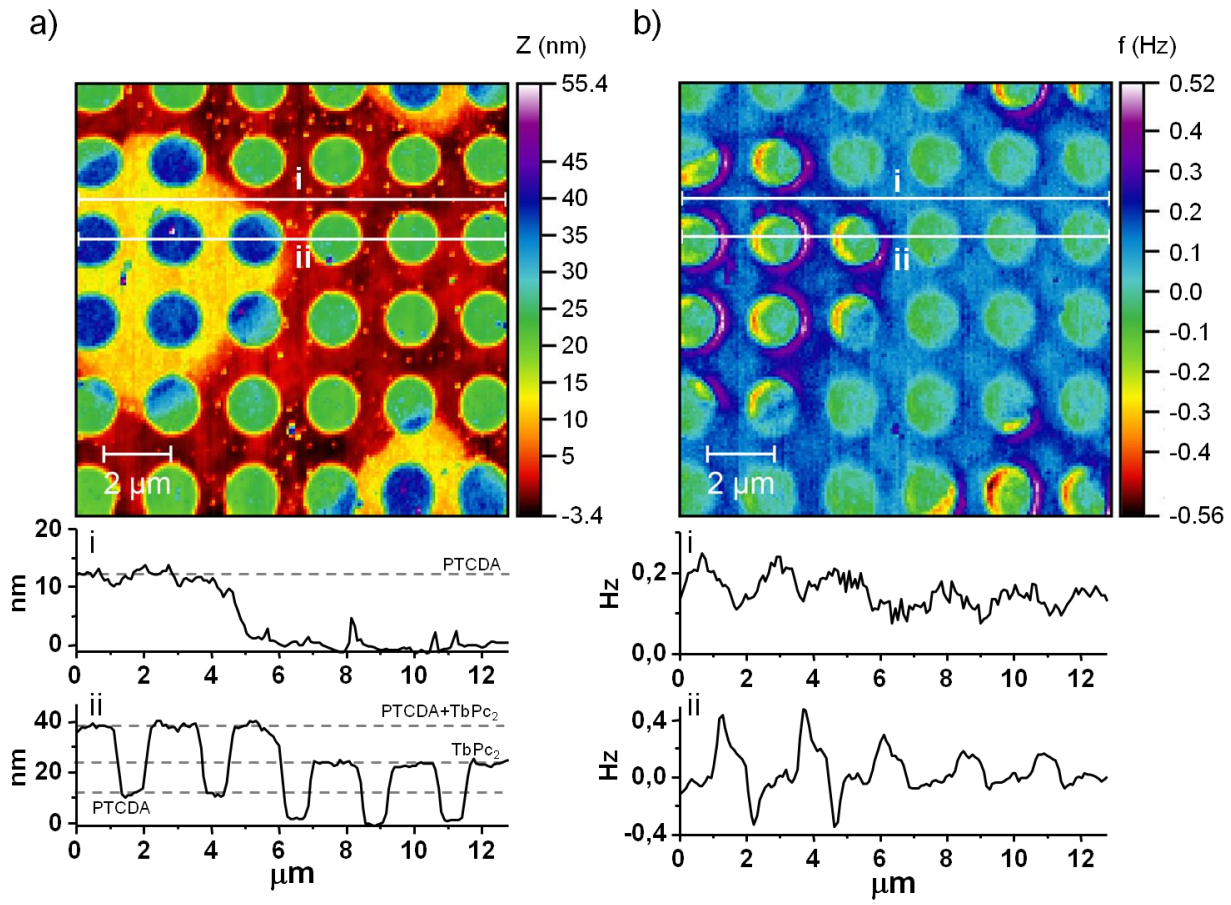


Figure 2 a) Topography of the $TbPc_2$ dot microarray on patterned PTCDA layer on silicon, measured at 10 K. The profiles along the lines i and ii are shown at the bottom, indicating that $TbPc_2$ structures are 24 nm thick, while PTCDA squares are 12 nm thick; the approximate heights of the structures are indicated with dashed lines. b) MFM image at a lift height of 85 nm from the surface, measured together with a) at 10 K and 4 Tesla. The MFM frequency shift profiles along the same i and ii lines measured in the topography are shown at the bottom.

The MFM signal on the templated areas show a peculiar crescent shaped distribution, which was further studied with high resolution images of an individual dot on PTCDA (Figure 3a and 3b); the observed crescent pattern was not dependent on the scanning direction or angle.

Similar high resolution images of a dot on silicon are shown in the supplementary information (Figure S3 in SI). Despite the near perfect axial symmetry of the structure, evident in the topography image (Figure 3a) and in the height profiles extracted along the vertical and the horizontal diameters, the magnetic image is only symmetric with respect to the horizontal diameter, as shown in Figure 3b and the line profiles. Repulsive forces (positive frequency shifts) are measured outside the right half of the dot, and attractive ones (negative shifts) on top of the left rim of the dot; the particle visible in the vertical line profile of the topography, which could be debris transported by the tip, is not giving a noticeable magnetic contribution.

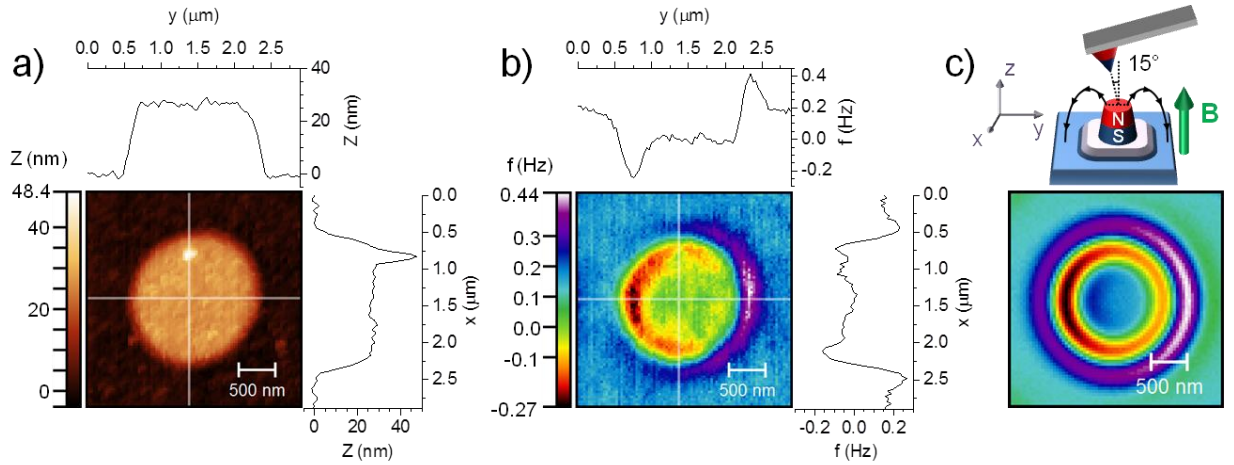


Figure 3 a) Topography image of a single $TbPc_2$ dot on PTCDA and profiles along the horizontal and vertical diameters, following the lines highlighted in the image. b) MFM image of the dot measured at 85 nm lift height and profiles along the lines highlighted in the image. c) Schematics of the MFM measurement geometry (top), indicating the 15° probe tilt angle and suggesting the origin of the anisotropic signal distribution, and simulated MFM image of a $TbPc_2$ dot at saturation (bottom) reproducing the crescent shaped signal distribution seen in the experiments. Details about the simulation are given in the experimental section in SI.

This distribution indicates that the magnetic moments of the sample and the tip are not collinear and, because of the perpendicular magnetization of $TbPc_2$ on PTCDA,[41] we conclude that it is due to the design of the microscope used in this study, where the MFM probe is mounted at a tilt angle of 15° with respect to the sample normal and the magnetic field direction, as schematically shown at the top of Figure 3c. This effect is probably reinforced by the strong anisotropy of the MFM tips used here (CoPt/FePt), which are likely to magnetize along the tip axis rather than the field direction, as well as by the relatively sharp edges of the truncated cone structures which result in a highly pronounced spatial dependence of the demagnetizing field. These distinctive features of our experiment may explain why this effect has not been observed in a similar study of $Gd(ac)_2$ microdots.[31] In support of this interpretation, we show at the bottom of Figure 3c a simulation of the magnetic force gradient, proportional to the MFM signal, calculated on a saturated $TbPc_2$ dot at an angle of 15° from the normal (details in the experimental section, see SI).The simulated image reproduces the crescent shaped features of the MFM image, although the magnetic point dipole tip model used in the calculation also predicts features that are likely averaged out by finite size of the probe used experimentally (nominal radius 32±7 nm). By using a more detailed model of the tip magnetization, or by calibrating the tip response,[45,46] one should be able to obtain a better qualitative agreement with the experimental image and, more importantly, to quantitatively assess the local magnetization distribution in the sample.

A simpler $TbPc_2$ microarray, containing dots 50 nm high grown on a continuous 20 nm PTCDA layer on silicon, has been prepared (see Figure S1 in SI). On this sample an extra characterization has been performed by Time of Flight Secondary Ion mass spectrometry (ToF-SIMS) in order to carefully evaluate the chemical distribution of the two species and the

presence of intact SMM; the spatial distribution of the detected molecular peak of $TbPc_2$ and PTCDA in the sample, reported in Figure S1, further confirmed the quality of the sample.
The field dependence of the MFM signal was studied at 5.9 K in these microarrays of $TbPc_2$. Crescent shaped features, analogous to those previously discussed, were observed with 3 T at a probe lift height of 71 nm (Figure 4a). In this second set of measurements performed again in dual pass mode, the lift height was further optimized and slightly decreased to further enhance the sensitivity to magnetic signal still minimizing the contribution due to short range interactions. The magnetic contrast showed a marked field dependence which is highlighted by the series of images shown in Figure 4c, measured between 3 T and -3 T. At fields above the coercivity of the tip both the tip and the sample are magnetized in the same direction, giving rise to MFM contrast insensitive to the field sign. An inversion of the contrast is expected when only one of the two interacting elements, the tip and the sample, has inverted its magnetization; however, this was not evident in our measurement due to the weakness of the signal at low field. Contrary to previous data, a small residual signal was detected in zero magnetic field (figure 4d-1), which may have a topographic origin, due to the shorter tip sample distance used in this measurement, or may be caused by an inhomogeneous surface potential[47] or an incomplete demagnetization of the magnet.

With the aim of extracting the magnetization curve of a single dot from MFM images, we developed an original method to analyze the MFM data, based on the partition of the image into three regions. These correspond to the areas where the tip experiences: (A) the strongest attractive forces (red colored crescent in the left half of the dot), (B) moderate attractive interaction (the yellow-green zone inside the dot), and (C) the strongest repulsive forces (purple colored crescent outside the right half of the dot). A set of three data-masks named A, B and C

(Figure 4b), defining the three regions, has been created with an algorithm (see experimental section in SI for details) starting from the image measured at 3 T, which has the strongest magnetic signal. When an external field is applied along an easy direction, as in the case of the $TbPc_2$ dots on PTCDA, the stray field of the sample should not change its spatial distribution but only its magnitude, hence it is legitimate to use the data-masks obtained at 3 T on images acquired at different fields. MFM images were aligned with the one at 3 T using the respective topography as reference. Then, on each image, the distribution of the resonance frequency shift values f respect to the initial one (f_0) in each of the three regions of the image was fitted with a Gaussian peak, obtaining a triad of peak positions (f_A, f_B, f_C) and widths (σ_A,σ_B ,σ_C), representing respectively the characteristic frequency shift and the spread of values in each of the three regions. The distance between any pair of peaks i, j ($\Delta f_{i,j}= f_i-f_j$) measures the variation of the force gradient between the regions i and j, which is proportional to the magnetization of the dot, while the sum of the widths of the peaks in the selected pair ($\sigma_i+\sigma_j$) was used to evaluate the uncertainty in the measurement, which depends both on the experimental noise and the choice of the masks. The f_C and f_A components, which correspond to the regions of maximum repulsive and attractive interaction, provided the lowest relative error and were used to construct the single dot magnetization curve shown in Figure 4e, to be compared to the hysteresis loop measured by XMCD. Both curves were normalized to the value measured at saturation (B=3T). The values obtained by MFM are shown as black spheres, numbered to express the measurement sequence. Since the tip magnetization follows the sign of the field above its coercivity, the MFM values measured at negative field have been multiplied by -1 for a better comparison with the XMCD data; the original values are also shown in blue color.

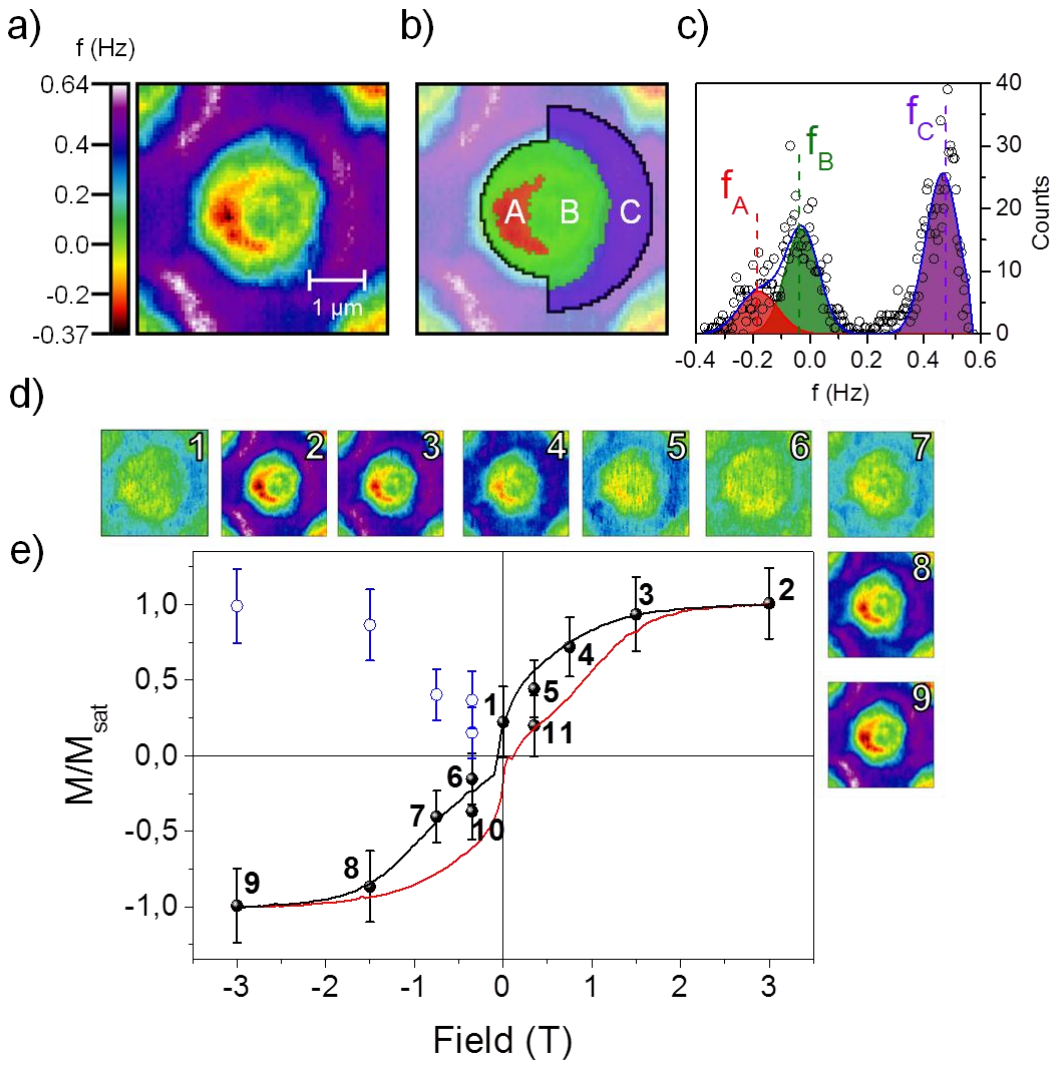


Figure 4 a) MFM image of a 50 nm thick $TbPc_2$ dot on a continuous (20 nm) PTCDA layer at 5.9 K, measured at a lift height of 71 nm. b) Overlay of a) with the data masks A, B, C that define the 3 regions used to evaluate the MFM contrast. c) Distribution of *f* values inside the region A+B+C. The distribution is fitted with three Gaussian peaks centered at f_A, f_B, f_C. d) MFM images (4.5 × 4.5 μm^2) of the dot as a function of field, shown with the same color scale range of the image reported in (a): (1) 0 T, (2) 3 T, (3) 1.5 T, (4) 0.75 T, (5) 0.35 T, (6) -0.35 T, (7) -0.75 T, (8) -1.5 T, (9) -3 T. e) Field dependence of the MFM signal of the $TbPc_2$ dot on PTCDA, defined as $\Delta f_{C,A} = f_C - f_A$, shown as spheres with error bars, and XMCD hysteresis curve of $TbPc_2$

film on PTCDA (20 nm $TbPc_2$/PTCDA film at 7 K, red indicate up sweep of the field, black down sweep); values are normalized by dividing by the saturation value at 3T. Black spheres display MFM contrast values with the same sign of the applied field, while blue spheres in the second quadrant show the normalized $\Delta f_{C,A}$ value; points are numbered to indicate the order of the measurements.

The resulting frequency shifts extracted from each MFM measurement at different fields, with their error bars, show good agreement with the hysteresis loop measured by XMCD. The MFM points measured in the downward and the upward field sweep seem to follow slightly different curves, suggesting the observation of a magnetic hysteresis. Though qualitatively in agreement with the butterfly hysteretic behavior detected by XMCD, the MFM detected bistability will require future additional investigations, being the differences small when compared to the error bars and, in the low field region, convoluted with the tip hysteretic behavior. Furthermore, the timescale of an MFM-detected magnetization measurement, which takes place in hours, is significantly longer than the one employed in synchrotron experiments that have been carried out at T=7 K. The lower temperature used in MFM test is expected to slightly increase the opening of the hysteresis cycle thus suggesting that lower temperature experiments should to be performed in the future even if the effect of resonant quantum tunneling occurring in $TbPc_2$ systems can limit this strategy.

In conclusion, our parallel investigation based on synchrotron radiation and magnetic force microscopy showed that the single molecule magnet properties of thin films of $TbPc_2$ can be greatly improved when the orientation of the anisotropy axis is controlled via a templating

layer of PTCDA. The hysteresis loop of the templated film shows in the XMCD measurement a wider opening than previously observed in monolayers deposited on Au(111)[35] and HOPG,[9] which exhibit a molecular orientation similar to the films on PTCDA considered here. This result is in line with the recent reports[36] showing that the addition of an insulating decoupling layer between $TbPc_2$ and a metallic substrate improves the spin relaxation times. PTCDA is not insulating and exhibits a n-type semiconductor behavior,[48] however its interaction with the SMM is expected to be much weaker than in the case of a metallic substrate, hence the reduction of the spin relaxation rate and the widening of the hysteresis.

The control of the orientation of the SMMs has allowed the patterning of a superstructure of the molecular film with dots presenting different orientation of the magnetization. This novel procedure allows to clearly disentangle topographic and magnetic signals significantly improving the reliability of the MFM analysis. The very good agreement of the magnetic data obtained by MFM with the hysteresis curve measured in fast sweep mode by XMCD points to the validity of this scanning probe technique for the local characterization of a single micrometric dot of a molecular magnet. The convolution of SMM and tip magnetic responses at low field is likely to be resolved by using probes of different coercivity, possibly allowing the imaging of the SMM hysteresis. Moreover, the innovative MFM image analysis presented here is expected to have a better statistical significance than the commonly used line profile method, since it takes into account larger regions of the image. Furthermore we believe that it can be easily adapted to perform *in line* analyses on SMM structures grown on top of nanostructured architectures during the realization of SMM-based devices, where it will be crucial to have a local knowledge of SMM properties such as the orientation of the anisotropy and the presence of magnetic bistability.

ASSOCIATED CONTENT

Supporting Information. The Supporting Information is available free of charge on the ACS Publications website at DOI: 10.1021/XXXXXXX. Experimental and methodologic information on $TbPc_2$ synthesis and sample preparation, shadow masking-based deposition details, AFM characterizations, ToF-SIMS analysis, XAS/XMCD experiment details, and MFM image simulations method.

AUTHOR INFORMATION

Corresponding Author

*matteo.mannini@unifi.it .

Present Addresses

† 1 CNRS, ICMCB, UPR 9048, F-33600 Pessac, France; 2 Univ. Bordeaux, ICMCB, UPR 9048, F-33600 Pessac, France

Author Contributions

The manuscript was written through contributions of all authors. MM, MS and RS designed the project. DR made the synthesis and MS prepared the nanostructured samples. BC, MM and MS developed the shadow masking deposition setup. MM, LP, MS, EVF, RS and PS performed the synchrotron experiments. MS and MM performed MFM experiments and developed the data analysis protocol. All authors have given approval to the final version of the manuscript.

Funding Sources

The financial support of the European Research Council through the Advanced Grant n. 267746 MolNanoMaS and EC through FP7-People-2011-IAPP (286196) ESN-STM are acknowledged. The support of Ente Cassa di Risparmio di Firenze to CeTeCS (Centro per le Tecniche di Caratterizzazione a Scansione di Sonda) is also acknowledged.

ACKNOWLEDGMENT

XMCD experiments were performed on beamline ID32 at the European Synchrotron Radiation Facility (ESRF), Grenoble, France. We are grateful to Dr. S. Heutz for approaching us to the use of templating agents, A. Fondacaro (ESRF) for providing assistance in using beamline ID32, Prof. A. Magnani (University of Siena) for the ToF-SIMS setup access, and to Dr. L. Malavolti for helpful discussion.

ABBREVIATIONS

LT-MFM, low temperature magnetic force microscopy; XMCD, X-ray magnetic circular dichroism; $TbPc_2$, terbium bisphthalocyaninato; PTCDA, Perylene-3,4,9,10-tetracarboxylic dianhydride.

REFERENCES

(1) Urdampilleta, M.; Klyatskaya, S.; Cleuziou, J.-P.; Ruben, M.; Wernsdorfer, W. *Nat. Mater.* **2011**, *10*, 502–506.

(2) Katoh, K.; Komeda, T.; Yamashita, M. *Dalt. Trans.* **2010**, *39*, 4708–4723.

(3) Malavolti, L.; Poggini, L.; Margheriti, L.; Chiappe, D.; Graziosi, P.; Cortigiani, B.; Lanzilotto, V.; Buatier de Mongeot, F.; Ohresser, P.; Otero, E.; Choueikani, F.; Sainctavit, P.; Bergenti, I.; Dediu, V. A.; Mannini, M.; Sessoli, R. *Chem. Commun. (Camb).* **2013**, *49*, 11506–11508.

(4) Mannini, M.; Pineider, F.; Sainctavit, P.; Danieli, C.; Otero, E.; Sciancalepore, C.; Talarico, A. M.; Arrio, M.-A.; Cornia, A.; Gatteschi, D.; Sessoli, R. *Nat. Mater.* **2009**, *8*, 194–197.

(5) Mannini, M.; Bertani, F.; Tudisco, C.; Malavolti, L.; Poggini, L.; Misztal, K.; Menozzi, D.; Motta, A.; Otero, E.; Ohresser, P.; Sainctavit, P.; Condorelli, G. G.; Dalcanale, E.; Sessoli, R. *Nat. Commun.* **2014**, *5*, 4582.

(6) Perfetti, M.; Pineider, F.; Poggini, L.; Otero, E.; Mannini, M.; Sorace, L.; Sangregorio, C.; Cornia, A.; Sessoli, R. *Small* **2014**, *10*, 323–329.

(7) Bogani, L.; Cavigli, L.; Gurioli, M.; Novak, R. L.; Mannini, M.; Caneschi, A.; Pineider, F.; Sessoli, R.; Clemente-León, M.; Coronado, E.; Cornia, A.; Gatteschi, D. *Adv. Mater.* **2007**, *19*, 3906–3911.

(8) Gonidec, M.; Davies, E. S.; McMaster, J.; Amabilino, D. B.; Veciana, J. *J. Am. Chem. Soc.* **2010**, *132*, 1756–1757.

(9) Klar, D.; Candini, A.; Joly, L.; Klyatskaya, S.; Krumme, B.; Ohresser, P.; Kappler, J.-P.; Ruben, M.; Wende, H. *Dalt. Trans.* **2014**, *43*, 10686–10689.

(10) Malavolti, L.; Lanzilotto, V.; Ninova, S.; Poggini, L.; Cimatti, I.; Cortigiani, B.; Margheriti, L.; Chiappe, D.; Otero, E.; Sainctavit, P.; Totti, F.; Cornia, A.; Mannini, M.; Sessoli, R. *Nano Lett.* **2015**, *15*, 535–541.

(11) Pietzsch, O.; Kubetzka, A.; Bode, M.; Wiesendanger, R. *Science (80-.).* **2001**, *292*, 2053–2056.

(12) Iacovita, C.; Rastei, M. V; Heinrich, B. W.; Brumme, T.; Kortus, J.; Limot, L.; Bucher, J.

P. *Phys. Rev. Lett.* **2008**, *101*, 116602.

(13) Schwöbel, J.; Fu, Y.; Brede, J.; Dilullo, A.; Hoffmann, G.; Klyatskaya, S.; Ruben, M.; Wiesendanger, R. *Nat. Commun.* **2012**, *3*, 953.

(14) Chen, X.; Fu, Y.-S.; Ji, S.-H.; Zhang, T.; Cheng, P.; Ma, X.-C.; Zou, X.-L.; Duan, W.-H.; Jia, J.-F.; Xue, Q.-K. *Phys. Rev. Lett.* **2008**, *101*, 197208.

(15) Tsukahara, N.; Noto, K.; Ohara, M.; Shiraki, S.; Takagi, N.; Takata, Y.; Miyawaki, J.; Taguchi, M.; Chainani, A.; Shin, S.; Kawai, M. *Phys. Rev. Lett.* **2009**, *102*, 167203.

(16) Kirtley, J. R.; Ketchen, M. B.; Stawiasz, K. G.; Sun, J. Z.; Gallagher, W. J.; Blanton, S. H.; Wind, S. J. *Appl. Phys. Lett.* **1995**, *66*, 1138.

(17) Chang, A. M.; Hallen, H. D.; Harriott, L.; Hess, H. F.; Kao, H. L.; Kwo, J.; Miller, R. E.; Wolfe, R.; van der Ziel, J.; Chang, T. Y. *Appl. Phys. Lett.* **1992**, *61*, 1974.

(18) Hehn, M.; Padovani, S.; Ounadjela, K.; Bucher, J. P. *Phys. Rev. B* **1996**, *54*, 3428–3433.

(19) Bochi, G.; Hug, H. J.; Paul, D. I.; Stiefel, B.; Moser, A.; Parashikov, I.; Güntherodt, H.-J.; O'Handley, R. C. *Phys. Rev. Lett.* **1995**, *75*, 1839–1842.

(20) Mamin, H. J.; Rugar, D.; Stern, J. E.; Fontana, R. E.; Kasiraj, P. *Appl. Phys. Lett.* **1989**, *55*, 318.

(21) Landis, S.; Rodmacq, B.; Dieny, B. *Phys. Rev. B - Condens. Matter Mater. Phys.* **2000**, *62*, 12271–12281.

(22) Zhu, X.; Grütter, P. *MRS Bull.* **2004**, *29*, 457–462.

(23) Chen, G.; Bodnarchuk, M. I.; Kovalenko, M. V; Springholz, G.; Heiss, W.; Jantsch, W.; Platzgummer, E.; Loeschner, H.; Schotter, J. *Adv. Mater.* **2010**, *22*, 1364–1368.

(24) Moser, A.; Hug, H. J.; Stiefel, B.; Gu, H. *J. Magn. Magn. Mater.* **1998**, *190*, 114–123.

(25) Volodin, A.; Temst, K.; Bruynseraede, Y.; Van Haesendonck, C.; Montero, M. I.; Schuller, I. K.; Dam, B.; Huijbregtse, J. M.; Griessen, R. *Phys. C Supercond.* **2002**, *369*, 165–170.

(26) Auslaender, O. M.; Luan, L.; Straver, E. W. J.; Hoffman, J. E.; Koshnick, N. C.; Zeldov, E.; Bonn, D. a.; Liang, R.; Hardy, W. N.; Moler, K. a. *Nat. Phys.* **2008**, *5*, 35–39.

(27) Tanaka, M.; Saito, Y.; Nishide, H. *Chem. Lett.* **2006**, *35*, 1414–1415.

(28) Cavallini, M.; Gomez-Segura, J.; Ruiz-Molina, D.; Massi, M.; Albonetti, C.; Rovira, C.; Veciana, J.; Biscarini, F. *Angew. Chem. Int. Ed. Engl.* **2005**, *44*, 888–892.

(29) Tangoulis, V.; Skarlis, M.; Raptopoulou, C. P.; Psycharis, V.; Dendrinou-Samara, C. *Eur. J. Inorg. Chem.* **2014**, *2014*, 2678–2686.

(30) Miyasaka, B. M.; Saito, Y.; Nishide, H. **2003**, No. 2, 113–117.

(31) Lorusso, G.; Jenkins, M.; González-Monje, P.; Arauzo, A.; Sesé, J.; Ruiz-Molina, D.; Roubeau, O.; Evangelisti, M. *Adv. Mater.* **2013**, *25*, 2984–2988.

(32) Pinilla-Cienfuegos, E.; Kumar, S.; Mañas-Valero, S.; Canet-Ferrer, J.; Catala, L.; Mallah, T.; Forment-Aliaga, A.; Coronado, E. *Part. Part. Syst. Charact.* **2015**, 693–700.

(33) Pinilla-Cienfuegos, E.; Mañas-Valero, S.; Forment-Aliaga, A.; Coronado, E. *ACS Nano* **2016**, *10*, 1764–1770.

(34) Ghirri, A.; Candini, A.; Evangelisti, M.; Gazzadi, G. C.; Volatron, F.; Fleury, B.; Catala, L.; David, C.; Mallah, T.; Affronte, M. *Small* **2008**, *4*, 2240–2246.

(35) Margheriti, L.; Chiappe, D.; Mannini, M.; Car, P. E.; Sainctavit, P.; Arrio, M. A.; De Mongeot, F. B.; Cezar, J. C.; Piras, F. M.; Magnani, A.; Otero, E.; Caneschi, A.; Sessoli, R. *Adv. Mater.* **2010**, *22*, 5488–5493.

(36) Wäckerlin, C.; Donati, F.; Singha, A.; Baltic, R.; Rusponi, S.; Diller, K.; Patthey, F.; Pivetta, M.; Lan, Y.; Klyatskaya, S.; Ruben, M.; Brune, H.; Dreiser, J. *Adv. Mater.* **2016**, *28*, 5195–5199.

(37) Klar, D.; Klyatskaya, S.; Candini, A.; Krumme, B.; Kummer, K.; Ohresser, P.; Corradini, V.; de Renzi, V.; Biagi, R.; Joly, L.; Kappler, J.-P.; Del Pennino, U.; Affronte, M.; Wende, H.; Ruben, M. *Beilstein J. Nanotechnol.* **2013**, *4*, 320–324.

(38) Candini, A.; Klyatskaya, S.; Ruben, M.; Wernsdorfer, W.; Affronte, M. *Nano Lett.* **2011**, *11*, 2634–2639.

(39) Otomo, A.; Yokoyama, S.; Nakahama, T.; Mashiko, S. *Appl. Phys. Lett.* **2000**, *77*, 3881.

(40) Robaschik, P.; Fronk, M.; Toader, M.; Klyatskaya, S.; Ganss, F.; Siles, P. F.; Schmidt, O. G.; Albrecht, M.; Hietschold, M.; Ruben, M.; Zahn, D. R. T.; Salvan, G. *J. Mater. Chem. C* **2015**, *3*, 8039–8049.

(41) Perfetti, M.; Serri, M.; Poggini, L.; Mannini, M.; Rovai, D.; Sainctavit, P.; Heutz, S.; Sessoli, R. *Adv. Mater.* **2016**, *28*, 6946–6951.

(42) Kummer, K.; Fondacaro, A.; Jimenez, E.; Velez-Fort, E.; Amorese, A.; Aspbury, M.; Yakhou-Harris, F.; van der Linden, P.; Brookes, N. B. *J. Synchrotron Radiat.* **2016**, *23*,

464–473.

(43) Katoh, K.; Yoshida, Y.; Yamashita, M.; Miyasaka, H.; Isshiki, H.; Zhang, Y. F.; Komeda, T.; Yamagishi, M. *J. Am. Chem. Soc.* **2009**, No. Iii, 9967–9976.

(44) Dreiser, J. *J. Phys. Condens. Matter* **2015**, *27*, 183203.

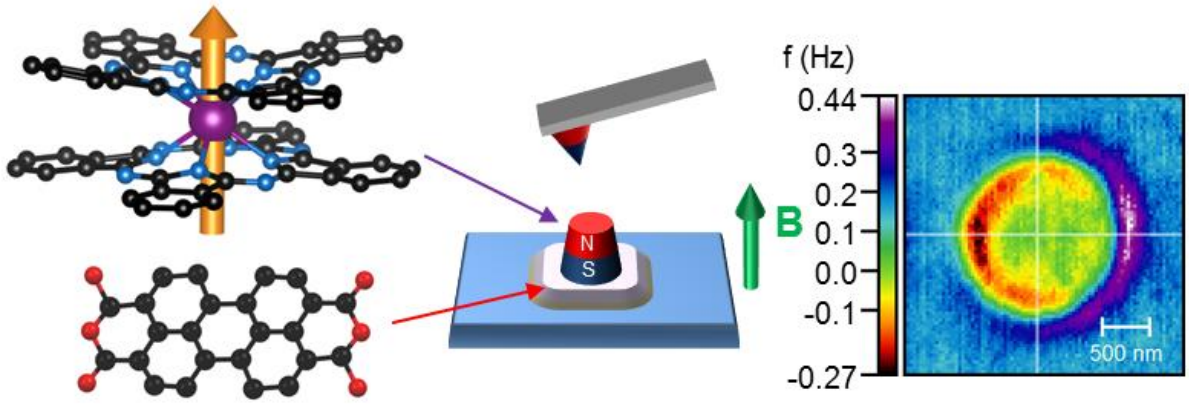
(45) Sievers, S.; Braun, K.-F.; Eberbeck, D.; Gustafsson, S.; Olsson, E.; Schumacher, H. W.; Siegner, U. *Small* **2012**, *8*, 2675–2679.

(46) van Schendel, P. J. A.; Hug, H. J.; Stiefel, B.; Martin, S.; Güntherodt, H.-J. *J. Appl. Phys.* **2000**, *88*, 435–445.

(47) Jaafar, M.; Iglesias-Freire, O.; Serrano-Ramón, L.; Ibarra, M. R.; de Teresa, J. M.; Asenjo, A. *Beilstein J. Nanotechnol.* **2011**, *2*, 552–560.

(48) Wuesten, J.; Ziegler, C.; Ertl, T. *Phys. Rev. B* **2006**, *74*, 125205.

Table of Contents Graphic and Synopsis



The local magnetic anisotropy and the field dependence of the magnetization of a specifically designed multilayered microarray structure including the Tb-double decker Single Molecule Magnet has been studied by low temperature magnetic force microscopy (LT-MFM) and results have been compared with X-ray magnetic circular dichroism data. An MFM-image analysis protocol for the extraction of magnetic information has been developed and proposed as a valuable tool for in line analysis of molecular or inorganic nanostructures.